An Integrated Approach to Modeling and Mitigating SOFC Failure
(Agreement No. DE-AC26-02NT41571)

Monthly Project Highlight Report

for the period of

February 1, 2003 – February 28, 2003

to

Don Collins
National Energy Technology Laboratory

From

PI: Jianmin Qu,
Co-PIs: Andrei Fedorov and Comas Haynes

School of Mechanical Engineering
Georgia Institute of Technology
801 Ferst Drive, N.W.
Atlanta, Georgia 30332-0405
Phone: 404-894-5687
FAX: 404-894-0186
E-Mail: jianmin.qu@me.gatech.edu

February 28, 2003

Agreement No.: DE-AC26-02NT41571

Reporting Period: – February 1, 2003 – February 28, 2003

Summary of Activities

Major activities of this month include

- Attendance and presentation at the SECA CTP Review meeting in Sacramento (CA) and discussion of the accomplished and future work with the Program Manager (Don Collins) and industrial partners from the vertical teams.
- Finished the investigation of the effect of thermal radiation on the local temperature fields in the SOFC. Developed a computationally efficient sub-module for solving a radiative transfer problem using the two-flux approximation. The module was integrated into the overall SOFC NETL FLUENT code and validated by comparing to the results with those obtained using the most accurate ,but computationally very expensive, discrete ordinate method.
- Initiated modeling efforts for mass transport in porous electrodes. Specifically, the theoretical formalism for treatment of mass transport via molecular diffusion, dispersion, Knudsen diffusion, and thermal diffusion (Soret effect) was developed.
- Developed a thermal shock model to understand the shock induced microcracks

Technical Highlights

Task 1: Fracture Mechanics Modeling

1.2 *Model Spalling Phenomenon and Thermal Expansion Induced Stress during Thermal Transients and Shock*

During start-up and shot-down, cells are subjected to thermal shocks. The rapid change of temperature can produce significant thermal stresses in the electrodes. If not managed properly, such thermal stresses may result in microcracks in the electrodes. The objective of this work is to develop a model to quantitatively understand how microcracks in the electrodes are created during transient thermal loading.

It was derived in Appendix A that microcrack density, Nb^3, in a material is related to the heating rate (Joule heating), q, through,

$$q = \frac{3\pi^2 k r_0}{2\alpha}\left[1+\frac{16(1-\nu^2)Nb^3}{9(1-2\nu)}\right]\sqrt{\frac{G_c\pi(1-\nu)}{E_0 b(1+\nu)}} \qquad (1.1)$$

where

E_0 = Elastic Young's modulus of the un-cracked material

ν = Poisson's ratio of the un-cracked material

G_c = Fracture toughness of the material

b = crack size

N = number of cracks per unit volume

k = Thermal diffusivity

α = Coefficient of linear thermal expansion

In the above, r_0 is a length parameter that characterizes the spatial non-uniformity of the heat source, see Eq. (A.4). Smaller r_0 means less uniform.

The following can be observed from (1.1).

(a) For a given material and spatial heat source distribution, the microcrack density is proportional to the heating rate. Furthermore, there seems to be a threshold value for heating rate

$$q_{th} = \frac{3\pi^2 k r_0}{2\alpha}\sqrt{\frac{G_c \pi(1-\nu)}{E_0 b(1+\nu)}} \tag{1.2}$$

below which the crack density is negligible. This threshold heating rate is proportional to the thermal conductivity, i.e., the faster thermal energy conducts through the heating area, the smaller the tendency of microcrack generation.

Table 1 Thermomechanical properties of Ni/YSZ

E(Pa)	ν	G_c (J/m^2)	k (J/(sec m K))	α (1/K)
96x10^9	0.3	9	5.84	12.22x10^{-6}

(b) The allocable heating rate is proportional to the square root of the materials fracture toughness. Shown in Fig. 1.1 is the relationship between fracture toughness and maximum allowable heating rate for various values of microcrack densities.

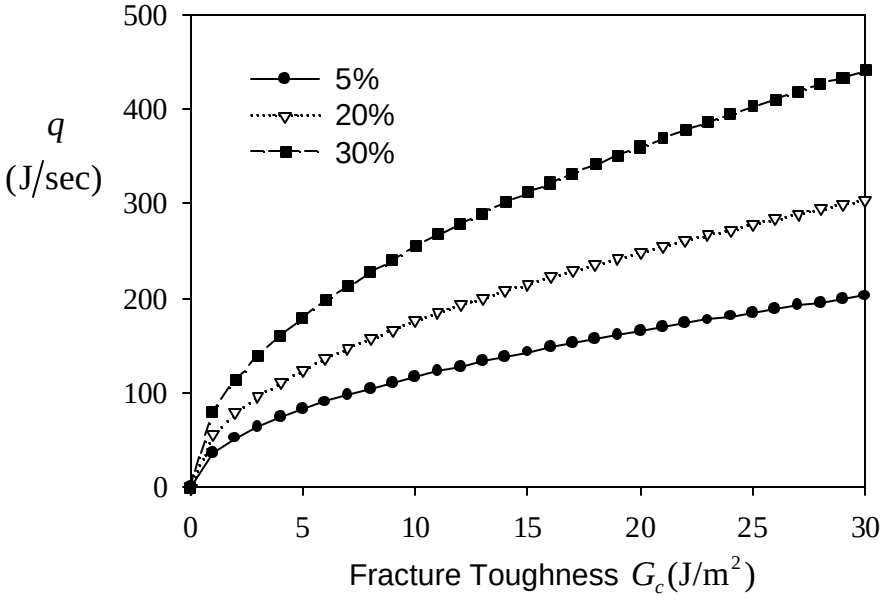

Fig. 1.1 Maximum allowable heating rate vs. fracture toughness

Task 2: Electrochemical Modeling

2.1 *Utilize/adapt existing electrochemical models, and develop enhancements necessary to achieve the project objectives and to advance the state-of-the-art.*

The validated electrochemistry model for the University of Utah anode-supported test SOFC (ref. January monthly report) was adapted from a structured-language platform to a graphical user-interface (GUI) that is relevant to the vertical teams. Primarily, the software tool is not computationally burdensome, but allows for near-real time evaluation of the impact of design conditions upon cell performance and reliability. Additionally, the dynamic, interactive interface is an effective means of establishing a "panoramic" view of the performance and reliability trade-offs associated with varying process conditions. A by-product is the increased intuition afforded an industrial researcher/designer. The primary enhancement thus achieved during this increment of the project is a feasible and viable means of aiding SOFC cell and stack design.

Task 3: Thermal Modeling

Figures 3.1a and 3.1b show the temperature variation along lines passing through the center of the cathode-electrolyte and the anode-electrolyte bi-layers, respectively, for the cases with and without inclusion of radiation effects. The radiation transfer is treated using the discrete ordinate method (the most accurate but computationally very expensive) as well as using the simplified two-flux approximation which is applicable for the optically thin electrolyte of SOFC. Radiation transfer in optically thick electrodes is simulated using Schuster-Shwarzchild's diffusion approximation, which is detailed in the previous reports. The representative optical properties of the electrodes and electrolyte are those obtained from the literature. As expected, inclusion of radiative transfer leads to a significant drop in the temperature level (by as much as 150^{o}C) which is accompanied by an increase in the cell voltage by almost 20%.

Further, we developed a computationally efficient sub-module for solving a radiative transfer problem using the two-flux approximation. The module was integrated into the overall NETL FLUENT code and validated by comparing to the results with those obtained using the most accurate, but computationally very expensive, discrete ordinate method. As it is indicated on Figs. 3.1a and b, the maximum difference between the temperature predictions obtained using the most accurate discrete ordinate (DO) method and the approximate two-flux method we used is less than 10^{o}C. At the same time, use of the two-flux approximation resulted in tremendous computational savings (by one order of magnitude) or reduction in CPU time from 658 minutes (DO method, FLUENT implementation) to just 76 minutes (two-flux approximation). The results of these calculations are supported by the previous independent study of Ceramatec (J. Hartvigsen, S. Elangovan, and A. Khandkar, ZIRCONIA V paper number 105).

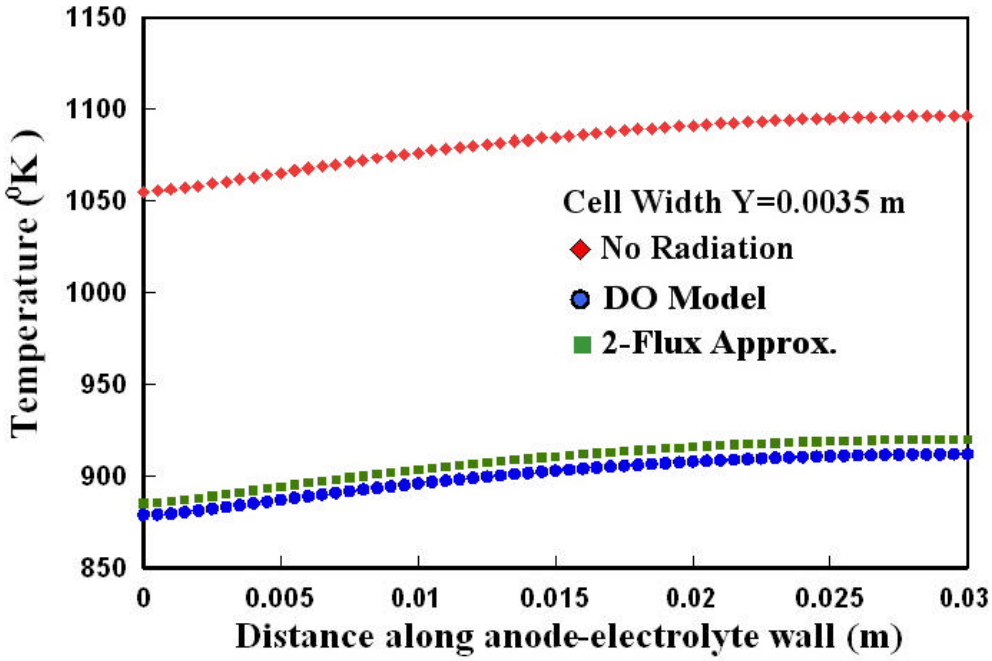

Fig. 3.1a: Effect of radiative transfer on the SOFC temperature (temperature along the anode-electrolyte interface)

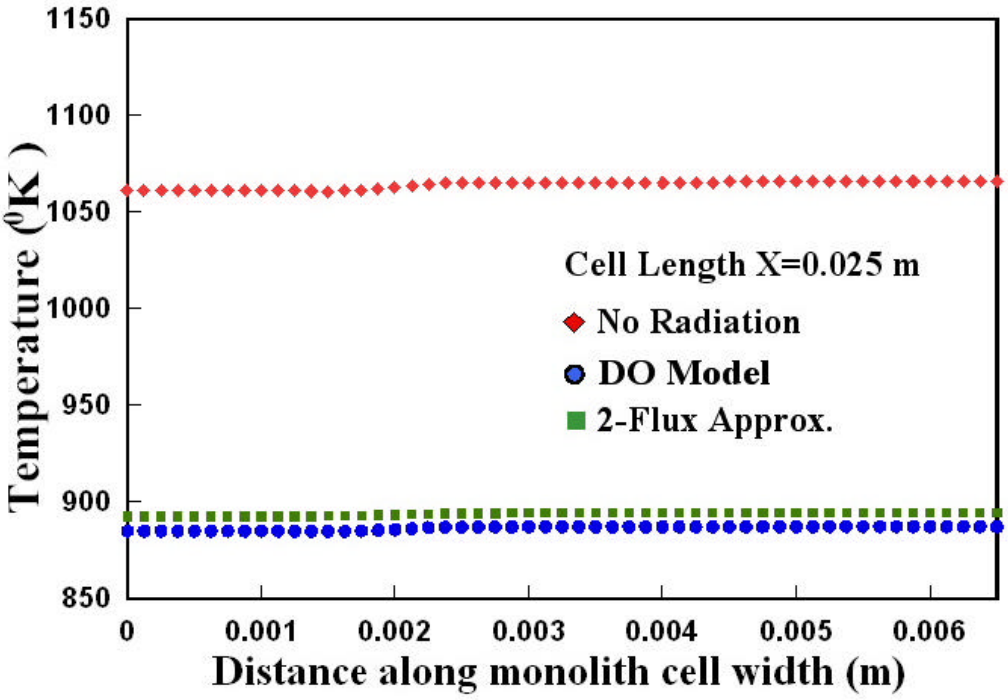

Fig. 3.1b: Effect of radiative transfer on the SOFC temperature (temperature along the cathode-electrolyte interface)

Numerical experiments are currently being carried out to study the effectiveness of the two-flux modeling scheme in capturing the radiation heat transfer process in the fuel cell. Simultaneously, efforts are also underway to address the convergence issues faced on inclusion of radiation in the solid electrolyte using the DO model.

Porous Media Mass Transport Modeling:

The species transport is governed by the following mass conservation equation:

$$\nabla \cdot \left(\rho \, \vec{V} \, Y_i \right) = \nabla \cdot \rho \left(D_i \, \nabla Y_i - D_{i,T} \frac{\nabla T}{T} \right) \pm S_i \tag{3.1}$$

where D_i and S_i refer to the effective diffusion coefficient and production/depletion rate of species i, respectively. While S_i is to be modeled through the chemistry/electrochemistry of relevant reactions, D_i has to be obtained by accounting for molecular diffusion, Knudsen diffusion, dispersion, and thermal diffusion effects.

$$D_i = \frac{\varepsilon}{\tau} \left(\frac{1 - \alpha_i \, x_i}{D_{i,m}} + \frac{1}{D_{i,K}} + \frac{1}{D_{i,d}} \right)^{-1} \tag{3.2}$$

Here, ε is the porosity, τ is tortuosity, x_i is the mole fraction of ith component, and $\alpha_i = 1 - \left(\frac{M_i}{M_m} \right)^{1/2}$ is the factor depending on the molar weights of the mixture components.

The molecular diffusion coefficient of the mixture can be expressed in terms of the pair-wise binary diffusion coefficients (D_{ik}) for the mixture components:

$$D_{i,m} = \frac{1-x_i}{\sum_{k\neq i}\frac{x_k}{D_{ik}}} \tag{3.3}$$

Because of the small diameter of the electrode pores, the Knudsen diffusion may be very significant as it specifies the resistance to the transport of a component due to ballistic molecule-pore walls collisions and needs to be included in the diffusion modeling of the porous electrodes. The Knudsen diffusion coefficient for i-th component of the mixture is expressed in terms of the mean pore radius (r), the universal gas constant (R), and the local absolute temperature (T) as follows:

$$D_{i,K} = \frac{2}{3}\left(\frac{8RT}{\pi M_i}\right)^{1/2} r \tag{3.4}$$

Further, the species dispersion due to local gradients in the flow velocity results in further enhancement of the mass transfer and can be accounted for by using, for example, the Taylor dispersion model in which the dispersion coefficient is expressed as a function of the local flow Peclet number and porosity ($D_{i,d} = f(Pe,\varepsilon)$).

Finally, the last term in the brackets accounts for the tendency of a component to diffuse under the influence of the temperature gradients across the electrodes in the fuel cell, known as the Soret effect. It can be captured through modeling the thermal diffusion effects. The thermal diffusion coefficient is expressed in terms of the local temperature (T), the molar weights (M_i), molar fractions (x_i), and mass fractions (y_i) of the mixture components.

$$D_{i,T} = -2.59\times10^{-7}T^{0.659}\left[\frac{M_i^{0.511}x_i}{\sum_{i=1}^{N}M_i^{0.511}x_i} - y_i\right]\bullet\left[\frac{\sum_{i=1}^{N}M_i^{0.511}x_i}{\sum_{i=1}^{N}M_i^{0.489}x_i}\right] \tag{3.5}$$

Our on-going efforts are focused on quantifying the relative importance of all of the above-mentioned effects on mass transport of reagents within the electrodes of the SOFC in order to identify the rate-limiting step under the various operating conditions and electrode designs.

Task 4: Multi-Physics Model Integration

Task 4.1: Review the implementation strategy of developed modeling modules within the PNNL/NETL simulation platform

Discussions with NETL/PNNL are on going to identify the best implementation strategy.

Task 4.2: Assess and identify areas within the PNNL/NETL simulation platforms where improvements will advance the state-of-the-art and contribute to the overall SECA Modeling and Simulation Program

Discussions with NETL/PNNL are on going to identify areas where improvements in are needed in the overall SECA Modeling and Simulation Program.

Completed Tasks

Tasks 2.3, 3.4 are complete, all others are on going.

Key Milestone Update

Tasks	Status	Remarks
1.1 Obtain fracture mechanics parameters for cohesive, interfacial and impinging cracks.	80% complete	
1.2 Model spalling phenomenon and thermal expansion induced stress during thermal transients and shock.	90% complete	
1.3 Identify and quantify crack path selection and crack propagation.	30% complete	
1.4 Implement temperature gradient as driving force for cracking. The Recipient shall investigate the individual and combined influences of electrochemical and mechanical load stress, as well as temperature gradients on crack initiation and propagation. The Recipient shall review and utilize/adapt, where appropriate, existing, available fracture mechanics models in order to advance the state-of-the-art.	0% complete	
1.5 Evaluate and validate the accuracy of developed fracture mechanics models using either experimental data or modeling results from PNNL/NETL/ORNL or other SECA members.	20% complete	
2.1 Utilize/adapt existing electrochemical models, and develop enhancements necessary to achieve the project objectives and to advance the state-of-the-art.	50% complete	
2.2 Models Extension to include porous electrode phenomena enhancements beyond the current state-of-the-art.	40% complete	
2.3 Evaluate and validate the accuracy of developed electrochemical models and enhancements using either experimental data or modeling results from PNNL/NETL/ORNL or other SECA members.	100% complete	

3.1 Formulation of 2-D and 3-D models for combined advection, conduction, and radiation heat and mass transfer in the porous electrodes.	90% complete	
3.2 Formulation of an approach for calculation of effective transport, thermophysical and radiative properties for the porous electrodes.	60% complete	
3.3 Formulation of coupled heat/mass transfer and electrochemistry model on the "unit-cell" level. The Recipient shall account for boundary effects, such as oxidant and fuel flow field channels, electrical interconnects and seals.	30% complete	
3.4 Review, select, and develop solution algorithms for numerical solution.	100% complete	
3.5 Evaluate and validate the accuracy of developed thermal models, algorithms and enhancements using either experimental data or modeling results from PNNL/NETL/ORNL or other SECA members.	20% complete	
4.1 Review the implementation strategy of developed modeling modules within the PNNL/NETL simulation platform.	50% complete	
4.2 Assess and identify areas within the PNNL/NETL simulation platforms where improvements will advance the state-of-the-art and contribute to the overall SECA Modeling and Simulation Program.	90% complete	

Discussion Topics

- As the team progresses through the project, it is becoming more imperative that a means of data exchange be established between the team and the vertical team "customers". Fortunately, the industry teams seemed amenable (and actually enthusiastic) to such dialogue and exchange. SECA program management is asked to help establish a coherent (i.e., systematic) means of communication between the two groups.

Significant Accomplishments

- Based on fracture mechanics, a thermal shock model was developed that can be used to estimate the maximum allowable heating rate, once the fracture toughness of the material is known.

- Finished the pilot demonstration of an engineering code, graphical user interface that allows for SECA industry teams to dynamically and interactively compare performance and reliability (via characterization of temperature non-uniformity) trends associated with pertinent process design variables. The tool was very well received by industry partners as a viable aid to their design efforts.
- Initiated modeling efforts for resolving the impact of process conditions (i.e., lite-off temperature, cell potential and fuel utilization) on rapid, yet safe, cell stack transitional heating during start-up.
- We developed a computationally efficient, and thus-far validated, sub-module for resolving electrochemical transport phenomena within SOFCs. The sub-module can be readily transported into a larger-scale systems design software such as ASPEN, wherein "top-down" systems-level design is facilitated so that SECA design goals/specs are reliably met.
- The graphical-user-interface provides a new paradigm for users to explore design feasibility and viability without being unnecessarily encumbered with either poorly simplistic or overwhelmingly complex graphical aids.
- The analysis of the effect of thermal radiation on the local temperature distribution inside of SOFC has been completed. The results indicate that significant errors may result in the local temperature (as much as 150 degrees Celsius) and especially local temperature gradients (responsible for crack formation) if the radiation effects are not properly accounted for.
- We developed a computationally efficient sub-module for solving a radiative transfer problem using the two-flux approximation. The module was integrated into the overall SOFC NETL FLUENT code and validated by comparing it to results obtained using the most accurate, but computationally very expensive, discrete ordinate method. The established computational methodology results in an accurate prediction of radiative transfer in SOFCs, and achieves such at one-order-of-magnitude lower computational cost as compared to standard discrete ordinate implementation.

Science & Technology Transfer

No science and technology transfer activities to report for this reporting period.

Presentations & Publications

Gave presentation on the progress at the SECA workshop in Sacramento, CA.

Site Visits

None to report for this reporting period.

Travel

Attended SECA workshop in Sacramento, CA.

Appendix A

Thermal Shock Induced Microcrack Initiation

We consider a body of infinite extent. The thermal elastic properties of the body are defined as follows:

E = Elastic Young's modulus

ν = Poisson's ratio

k = Thermal conductivity

κ = Thermal diffusivity

α = Coefficient of linear thermal expansion

ρ = Mass density

c = Specific heat capacity

If heat is liberated at the rate q_0 per unit time at the point $\mathbf{x}_1$, the temperature at $\mathbf{x}$ at time t is

$$T_0(\mathbf{x}, \mathbf{x}_1, t) = \frac{q_0}{4\pi\rho c\kappa r}\operatorname{erfc}\left(\frac{r}{\sqrt{4\kappa t}}\right) \tag{A.1}$$

where erfc(x) is the complimentary error function, and

$$r = |\mathbf{x} - \mathbf{x}_1| = \sqrt{r^2 + r_1^2 - 2rr_1\cos\varphi} \tag{A.2}$$

Now consider the case when heat is librated at the rate $q\rho c$ over the entire body with the spatial distribution

$$f(\mathbf{r}) = \frac{q}{\rho c\left(\sqrt{\pi}r_0\right)^3}\exp\left(-\frac{r^2}{r_0^2}\right) \tag{A.3}$$

The corresponding temperature distribution can be obtained by integrating (A.1),

$$T(\mathbf{x}, t) = \frac{q}{\rho c\left(\sqrt{\pi}r_0\right)^3}\iiint_{\infty}\frac{1}{4\pi\kappa|\mathbf{x} - \mathbf{x}_1|}\operatorname{erfc}\left(\frac{|\mathbf{x} - \mathbf{x}_1|}{\sqrt{4\kappa t}}\right)\exp\left(-\frac{|\mathbf{x}_1|^2}{r_0^2}\right)d\mathbf{x}_1 \tag{A.4}$$

To carry out the integral, consider

$$\frac{\partial T(\mathbf{x},t)}{\partial t}=\frac{q}{8\rho c\left(\pi r_0\sqrt{\kappa t}\right)^3}\iiint_{\infty}\exp\left(-\frac{|\mathbf{x}_1|^2}{r_0^2}-\frac{|\mathbf{x}-\mathbf{x}_1|^2}{4\kappa t}\right)d\mathbf{x}_1$$

$$=\frac{q}{8\rho c\left(\pi r_0\sqrt{\kappa t}\right)^3}\int_0^{\infty}\exp\left(-\frac{r_1^2}{r_0^2}\right)r_1^2\left[\int_0^{\pi}\exp\left(-\frac{r^2+r_1^2-2rr_1\cos\varphi}{4\kappa t}\right)\sin\varphi\, d\varphi\right]dr_1 \quad \text{(A.5)}$$

$$=\frac{q}{2\pi^2 r r_0^3\rho c\sqrt{\kappa t}}\int_0^{\infty}\left[\exp\left(\frac{rr_1}{\kappa t}\right)-1\right]\exp\left(-\frac{r_1^2}{r_0^2}-\frac{(r-r_1)^2}{4\kappa t}\right)r_1 dr_1$$

This integral can be carried out to yield the rate of temperature change

$$\dot{T}=\frac{\partial T(\mathbf{x},t)}{\partial t}=\frac{q}{\rho c\pi^{3/2}\left(r_0^2+4\kappa t\right)^{3/2}}\exp\left(\frac{-r^2}{r_0^2+4\kappa t}\right) \quad \text{(A.6)}$$

It can be shown that the maximum rate of temperature change occur at $t = 0$ and $r = 0$,

$$\dot{T}_{\max}\equiv\max\left\{\frac{\partial T(\mathbf{x},t)}{\partial t}\right\}=\frac{q}{\rho c\pi^{3/2}r_0^3} \quad \text{(A.7)}$$

The temperature is obtained by integrating (A.6),

$$T(r,t)=\frac{q}{4\pi r\rho c\kappa}\left[\operatorname{erf}\left(\frac{r}{r_0}\right)-\operatorname{erf}\left(\frac{r}{\sqrt{r_0^2+4\kappa t}}\right)\right]+T_0 \quad \text{(A.8)}$$

where T_0 is the initial (uniform) temperature of the body, and erf(x) is the error function.

In the spherical coordinate system (r,θ,φ), the non-zero stresses induced by a spherically symmetric temperature field $T(r,t)$ are given by

$$\sigma_r(r,t)=-\frac{2\alpha E}{1-\nu}\frac{1}{r^3}\int_0^r T(s,t)s^2 ds \quad \text{(A.9)}$$

$$\sigma_\theta(r,t)=\sigma_\varphi(r,t)=\frac{\alpha E}{1-\nu}\left[\frac{1}{r^3}\int_0^r T(s,t)s^2 ds-T(r,t)\right] \quad \text{(A.10)}$$

Substitution of (A.8) into (A.9) – (A.10) yields

$$\sigma_r(r)=\frac{-q\alpha E}{8\pi^{3/2}(1-\nu)r^3\rho c\kappa}\left[2rr_0e^{-r^2/r_0^2}+\sqrt{\pi}\,(2r^2-r_0^2)\operatorname{erf}\left(\frac{r}{r_0}\right)\right] \quad \text{(A.11)}$$

$$\sigma_\theta(r)=\sigma_\varphi(r)=\frac{q\alpha E}{18\pi^{3/2}(1-\nu)r^3\rho c\kappa}\left[-2rr_0e^{-r^2/r_0^2}+\sqrt{\pi}\,(2r^2+r_0^2)\operatorname{erf}\left(\frac{r}{r_0}\right)\right] \quad \text{(A.12)}$$

It can be easily shown that the stresses are a maximum at the center of the heating zone ($r = 0$), and decay rapidly away from it. The maximum values are

$$\sigma_r(0) = \sigma_\theta(0) = \sigma_\varphi(0) = \frac{-q\alpha E}{3\pi^{3/2}(1-\nu)\rho c\kappa r_0} \tag{A.13}$$

The corresponding mechanical strain (total strain minus the thermal strain) components can be computed from the Hooke's law

$$\varepsilon_r(0) = \varepsilon_\theta(0) = \varepsilon_\varphi(0) = \frac{-q\alpha(1-2\nu)}{3\kappa(1-\nu)\pi^{3/2} r_0} \tag{A.14}$$

The strain energy density near the heating center can then be computed from (A.13) – (A.14),

$$U_b = \frac{q^2\alpha^2 E(1-2\nu)}{6\rho^2 c^2\kappa^2(1-\nu)^2\pi^3 r_0^2} \tag{A.15}$$

Next, consider that, under this thermal shock, microcracks are formed near the heated center. Let the number of microcracks per unite volume be *N*. For simplicity, we assume all the microcracks are penny-shaped cracks with radius *b*. Due to the microcracks, the effective modulus of the material near the heating center changes. If all the microcracks are randomly oriented, the effective Young's modulus of the cracked body can be approximated by

$$E = E_0\left[1 + \frac{16(1-\nu^2)Nb^3}{9(1-2\nu)}\right]^{-1} \tag{A.16}$$

where E_0 is the Young's modulus of the un-cracked body.

The creation of microcracks reduces the amount of strain energy in the body. The amount of strain energy reduction should equal to the energy associated with all microcracks. Assuming the material in consideration is very brittle (no plastic deformation) and heat generation due to cracking is negligible, then the only energy associated with the creation of microcracks is the surface energy of the newly created crack surfaces,

$$U_s = 2\pi Nb^2\gamma \tag{A.17}$$

where γ is the surface energy per unit area of the material, which is related to fracture toughness G_c through

$$\gamma = \frac{1}{2}G_c = \frac{1-\nu^2}{2E}K_{Ic}^2 \tag{A.18}$$

The Griffith fracture criterion then requires

$$\frac{d(U_s + U_b)}{da} = 0 \tag{A.19}$$

This yields

$$q = \frac{3\pi^2 k r_0}{2\alpha}\left[1+\frac{16(1-\nu^2)Nb^3}{9(1-2\nu)}\right]\sqrt{\frac{2\gamma\pi(1-\nu)}{E_0 b(1+\nu)}} \tag{A.20}$$

or

$$q = \frac{3\pi^2 k r_0}{2\alpha}\left[1+\frac{16(1-\nu^2)Nb^3}{9(1-2\nu)}\right]\sqrt{\frac{G_c\pi(1-\nu)}{E_0 b(1+\nu)}} \tag{A.21}$$